Highly efficient flexible inverted organic solar cells using atomic layer deposited ZnO as electron selective layer

Jen-Chun Wang,[a] Wei-Tse Weng,[b] Meng-Yen Tsai,[c] Ming-Kun Lee,[b] Sheng-Fu Horng,*[b] Tsong-Pyng Perng,[a] Chi-Chung Kei,[c] Chih-Chieh Yu[c] and Hsin-Fei Meng[d]

Received 16th October 2009, Accepted 9th December 2009
First published as an Advance Article on the web 23rd December 2009
DOI: 10.1039/b921396a

With atomic-layer-deposition grown zinc oxide as the electron selective layer, we developed plastic substrate compatible processing for organic photovoltaic devices and demonstrated flexible inverted organic solar cells on poly(ethylene naphthalate) with a power conversion efficiency of 4.18%.

Organic photovoltaic (OPV) devices have attracted much attention due to their promising properties such as mechanical flexibility, light weight and potential low production cost. With various structure, material and process advancements, the power conversion efficiency (PCE) of organic solar cells (OSCs) has been improved significantly and exceeded 5%.[1,2] Current foci of OPV research include the development of low-bandgap polymers for better solar energy absorption, the improvement of longterm stability and processing steps as well as device structure suitable for cost-effective large-scale manufacturing.[3–6]

Conventional organic solar cells are often built on glass substrates which make the cells unsuitable for some applications such as smart cards, E-papers and ultra-thin watches. In addition, highly flexible substrates are well suited for high throughput continuous roll-to-roll manufacturing process which may greatly reduce the production cost. Thus, the development of organic solar cells on flexible substrates is a critical issue.

Conventional OSCs generally consist of an acidic poly(3,4-ethylenedioxythiophene) : poly(styrenesulfonate) (PEDOT : PSS) layer which is detrimental to the transparent conducting oxide (TCO) anode and a low work function metallic cathode which oxidizes easily in air. Therefore, these devices exhibit poor lifetimes.[7–9] In addition, it has been reported that the spontaneous phase separation of donor and acceptor in bulk heterojunction (BHJ) OSC exhibits higher concentration of acceptor at the TCO side. Such a vertical concentration distribution of donor and acceptor disfavors charge transport in the direction required in conventional OSC. An alternative solution is to use the inverted structure, with which the collecting nature of electrodes is reversed.[10–12]

In inverted organic solar cells, an interfacial layer such as caesium carbonate (Cs_2CO_3) is required to modify the polarity of TCO. With Cs_2CO_3, inverted OPV devices on glass with PCE more than 4% was demonstrated.[7] However, Cs_2CO_3 exhibits deliquescence which affects severely the lifetime of OPV devices.[13] Recently air stable zinc oxide (ZnO) has been introduced into OPV devices as the electron selective/hole blocking layer because of its high electron mobility. Kyaw *et al.* prepared a ZnO electron selective layer by a sol–gel process in an inverted OPV device on a glass substrate to achieve a PCE of 3.09%.[14] Hau *et al.* adopted spin-coated ZnO nanoparticles as the electron selective layer and maximum PCEs of 3.78% and 3.58% was achieved for inverted OPV devices fabricated on glass and plastic substrates, respectively.[15] Krebs employed solution processed ZnO in air-stable hybrid organic solar cells which require no vacuum processing steps and fullerenes.[16] In addition, solution processable ZnO was successfully applied to roll-to-roll processing of inverted OPV devices by Krebs *et al.*[17–19] The sol–gel process cannot be applied to flexible OPV devices on plastic substrate since the formation of ZnO films requires a high sintering temperature of more than 350 °C. Although solution-processed ZnO nanoparticles can be prepared at relatively low temperature, its properties depend strongly on the particle size and a precise control of the layer thickness is difficult.

ZnO can also be deposited with atomic layer deposition (ALD). ALD is a kind of chemical vapor deposition (CVD) technique with the precursor gas reactants being introduced into the reaction zone separately and sequentially.[20] Due to the self-limiting characteristic of the reaction between reactant gas and solid surface, conformal and pinhole-free films can be deposited layer by layer at atomic scale. Therefore, with ALD one has not only precise control over film thickness but also superior film quality. Recently, the ALD process has also been applied to the passivating encapsulation of organic devices.[21] Moreover, ZnO layer can be prepared by ALD at low temperatures and in large areas[22] and was shown to produce high quality hybrid diodes with poly(3-hexylthiophene) (P3HT).[23] Consequently, ALD-grown ZnO may be a promising candidate for electron selective layers in flexible OPV devices.

In this communication, ALD was employed to prepare a ZnO electron selective layer used in the inverted cell structure and the effects of layer thickness and substrate temperature were also investigated. With the ALD-grown ZnO electron selective layer in our flexible inverted OPV devices, a maximum PCE of 4.18% can be achieved.

Fig. 1(a) and (b) illustrate the device structure and band diagram of our inverted organic solar cells, respectively. ZnO was employed as the electron selective layer due to its high electron mobility. Since the valence band edge of ZnO is much lower than those of the highest occupied molecular orbitals (HOMOs) of both P3HT and [6,6]-phenyl C61 butyric acid methyl ester (PCBM), the ZnO layer serves

[a]*Department of Materials Science and Engineering, National Tsing Hua University, Hsinchu, 30013, Taiwan*
[b]*Institute of Electronics Engineering, National Tsing Hua University, Hsinchu, 30013, Taiwan. E-mail: sfhorng@itri.org.tw*
[c]*Instrument Technology Research Center, National Applied Research Laboratories, Hsinchu, 30013, Taiwan*
[d]*Institute of Physics, National Chiao Tung University, Hsinchu, 30013, Taiwan*

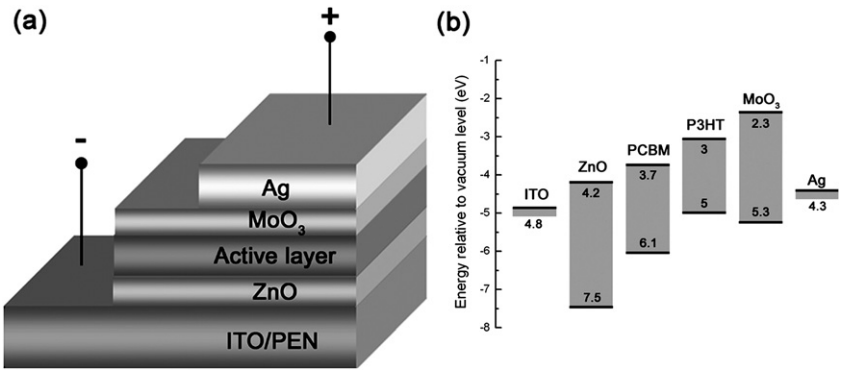

Fig. 1 (a) The device structure and (b) the energy band diagram of the flexible inverted organic solar cell investigated in this study.

also as a hole blocking layer. Similarly, the MoO_3 layer was used to block the electron flow because of its small electron affinity and to enhance hole transport to the anode, as reported in ref. 14.

To fabricate the device, indium tin oxide (ITO)-coated poly-(ethylene naphthalate) (PEN) substrates (15 Ω $\square^{-1}$, obtained from Peccell Technologies, Inc.) were first cleaned in an ultrasonic bath with detergent and de-ionized water for 10 min. ZnO thin films were then deposited by ALD, using diethyl zinc (DEZ) and water as the precursors. The pulse time of each reactant was set at 0.2 s, and a nitrogen purge with a moderate interval of time was introduced between the pulses of reactants to prevent CVD reaction in the vapor phase. Two different substrate temperatures of 45 °C (background temperature) and 80 °C were chosen, and the film thickness was controlled by the growth cycle number. The background temperature is higher than room temperature because the processing chamber and precursor pipelines have to be heated to avoid the condensation of precursors. Subsequently, a 1,2-dicholorobenzene (DCB) solution composed of P3HT (24 mg ml^{-1}, purchased from Rieke Metals) and PCBM (24 mg ml^{-1}, purchased from Nano-C) was spun onto the ZnO layer at 600 rpm. The devices were then annealed at 110 °C for 20 min and were then completed with sequent deposition of a 2 nm thick molybdenum trioxide (MoO_3) and an 80 nm thick Ag top electrode by thermal evaporation. The area of device is 4 mm^2. Except for the deposition condition of ZnO thin films, all the process parameters were fixed throughout the device fabrication process.

The current density–voltage (J–V) characteristics of the devices were measured with a Keithley 2400 source measurement unit using a 100 mW cm^{-2} AM 1.5G solar simulator (Peccell, PEC-L11). The illumination intensity was determined by a NREL calibrated Si detector with a KG-5 filter. The external quantum efficiency (EQE) was measured by a measurement system built up by Optosolar Inc. A 300 W Xe arc light source is coupled to a monochromator to obtain the required scanning light. A lock-in amplifier, which comes with a built-in chopper controller, was used to detect and measure small signals accurately from a calibrated Si detector over the 350–1160 nm spectral range. Surface roughness and morphology were characterized by atomic force microscopy (AFM, Veeco Dimension 3100) and scanning electron microscopy (SEM, Hitachi S-4300). Surface properties of the ZnO thin film were determined by contact angle measurement system (KRÜSS universal surface tester model GH-100).

Fig. 2 shows the XRD pattern of a ZnO thin film deposited at 45 °C with 400 ALD cycles on an ITO-coated PEN substrate. The first three diffraction peaks can be clearly observed and the (002) plane has a higher diffraction intensity, revealing a (002) direction preferred orientation. An SEM cross-section micrograph of the ZnO film is included as the inset in Fig. 2, exhibiting a uniform thickness around 72 nm.

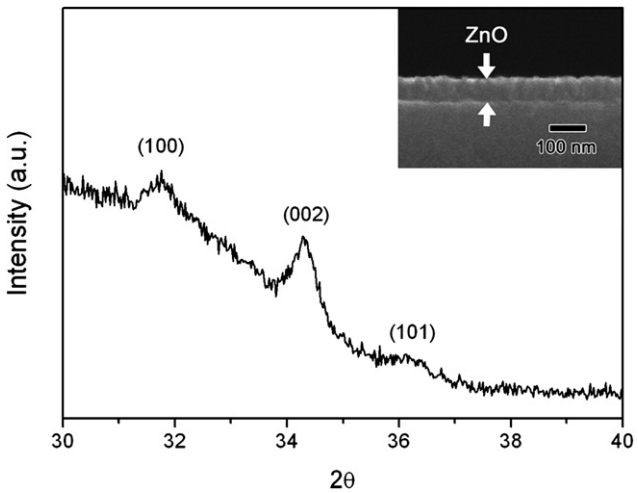

Fig. 2 The XRD pattern of a ZnO thin film deposited on a PEN/ITO substrate for 400 ALD cycles at 45 °C. The inset SEM micrograph shows the corresponding cross-sectional view of a thin film.

The illuminated current density-voltage (J–V) curves of devices with various ZnO thicknesses deposited at 45 °C are shown in Fig. 3(a). For better observation, the fourth quadrant of the J–V curve is expanded in Fig. 3(b). For the device without a ZnO layer, the current density rises at around $V = -0.2$ V and quickly increases as voltage increases, giving a small open-circuit voltage (V_{oc}) of 0.33 V. With the addition of 18 nm thick ZnO, the magnitude of the photocurrent increases and the rise of the current density is retarded, leading to an increased V_{oc} of 0.51 V. For the other three devices with thicker ZnO thin films, the current density shows normal diode-like characteristics and the V_{oc} remains constant at 0.59 V. The fill factor (FF), however, reaches a maximum of 0.56 at the thickness of 36 nm and gradually decreases as the thickness increases. Note that similar plateau features in the J–V curves, as shown in Fig. 3(a) for OSCs without and with 18 nm ZnO, were reported previously and were attributed to carrier transport problem.[24–26] It is also interesting to observe from Fig. 3(a) that the addition of 18 nm ZnO strongly reduces the current density in the first quadrant. As the ZnO

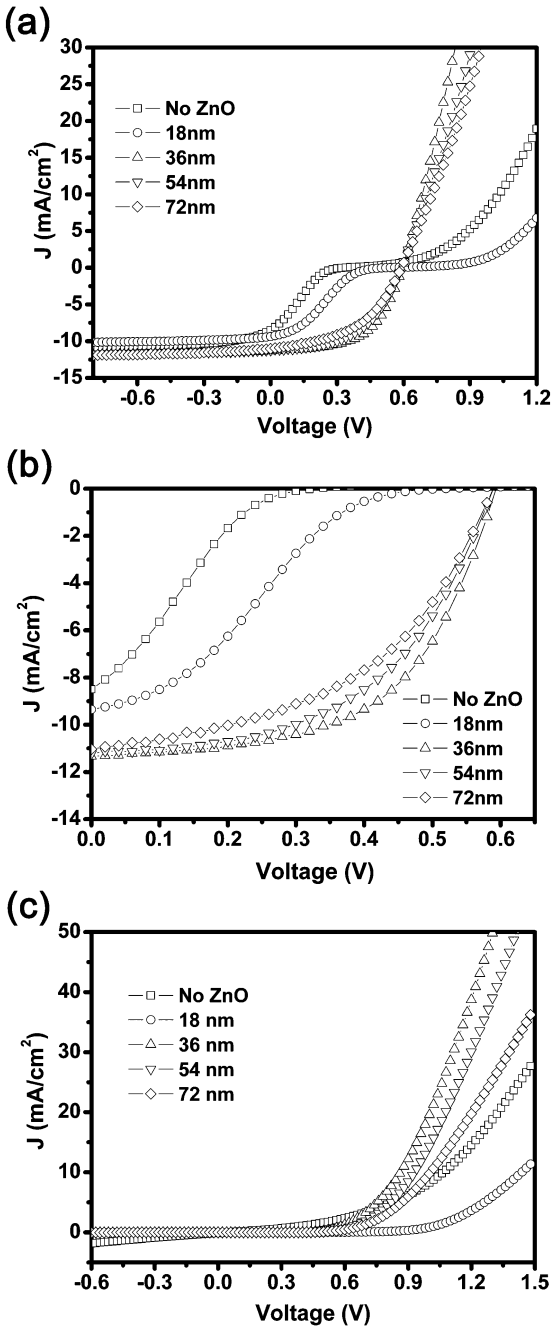

Fig. 3 The *J–V* characteristics of the inverted organic solar cells with different ZnO thicknesses deposited at 45 °C, (a) under AM 1.5G illumination, (b) expanded fourth quadrant with illumination, and (c) in the dark.

thickness further increases, the current density at a constant voltage in the first quadrant increases and then slightly decreases, similar to the *J–V* in the fourth quadrant. A similar trend with ZnO thickness was also observed from the dark *J–V*, as shown in Fig. 3(c). Because both V_{oc} and FF are significantly enhanced with the addition of ZnO, the PCE is also greatly enhanced. The performance parameters of these inverted OSCs with ZnO grown at 45 °C are summarized in Table 1.

The *J–V* curves can be understood by noting the dominant charge transport mechanisms in the solar cells. For the inverted solar cell without ZnO, the energy barrier height for electron (hole) injection

Table 1 Summary of the performance parameters of inverted organic solar cells with ZnO layer of different thickness grown at 45 °C by ALD process. 100 mW cm^{-2} AM 1.5G simulated solar illumination is used

ZnO thickness/nm	J_{SC}/mA cm^{-2}	V_{oc}/V	FF	η (%)
No ZnO	8.50	0.33	0.21	0.57
18 nm	9.35	0.51	0.26	1.24
36 nm	11.34	0.59	0.56	3.78
54 nm	11.20	0.59	0.52	3.41
72 nm	11.03	0.59	0.47	3.07

from ITO (Ag) into the active layer is 0.9 eV (1.0 eV). The dark carrier injection from the electrodes into the active layer is hence inhibited and the total current is determined by recombination among the photocarriers and the transport of the photocarriers in the active layer.[27] This is different from the case of organic solar cells with Ohmic contacts, for which the total current is dominated by recombination between the injected carriers and photocarriers. While the recombination among the photocarriers is relatively constant, the transport of photocarriers depends strongly on the bulk electric field. Because ITO has a larger work function than Ag, the flat-band condition is met at negative bias and hole transport to ITO is favored at non-negative voltage. Early rise of the current density and small V_{oc} are therefore expected. Only at sufficiently high bias can there be sufficient carrier injection from the electrodes into the active layer; the inverted solar cell without ZnO therefore exhibits a plateau feature as shown in Fig. 3(a).

With the addition of 18 nm ZnO, the hole transport to ITO is blocked and the bulk electric field is reduced, which favors the collection of electrons to ITO. Therefore, the rise of the total current, *i.e.*, the reduction in the magnitude of photocurrent, is retarded. Furthermore, the suppression of current at high forward bias reveals that the forward current is mostly due to hole transport, which is reasonable since MoO_3 serves as a buffer layer[28] that enhances hole injection from Ag/MoO_3 into the active layer at high forward bias. For the other devices with thicker ZnO, the collection of electrons to the ITO cathode is further enhanced by continued reduction of the bulk electric field. The creation of a potential well at the heterojunction between the ZnO conduction band and the active layer may also play a role. With increased ZnO thickness, the energy of the bottom in this potential well is reduced and electron accumulation is favored, which enhances the electron transport to ITO. The reduction

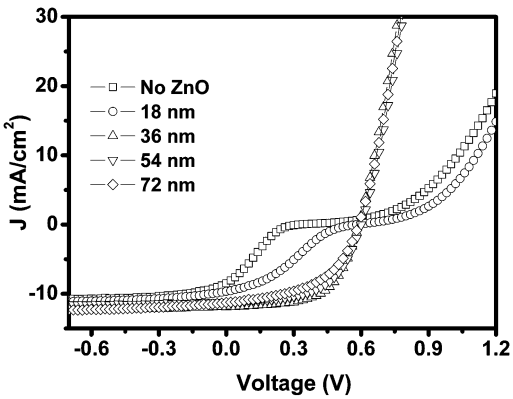

Fig. 4 The *J–V* characteristics of the inverted organic solar cells with different ZnO thicknesses deposited at 80 °C under AM 1.5 G illumination.

Table 2 Summary of the performance parameters of inverted organic solar cells with ZnO layer of different thickness grown at 80 °C by ALD process. 100 mW/cm^2 AM1.5G simulated solar illumination is used

ZnO thickness/nm	J_{SC}/mA cm^{-2}	V_{oc}/V	FF	η (%)
No ZnO	8.50	0.33	0.21	0.57
18 nm	9.65	0.59	0.29	1.61
36 nm	11.90	0.59	0.60	4.18
54 nm	11.20	0.60	0.57	3.69
72 nm	11.30	0.59	0.50	3.35

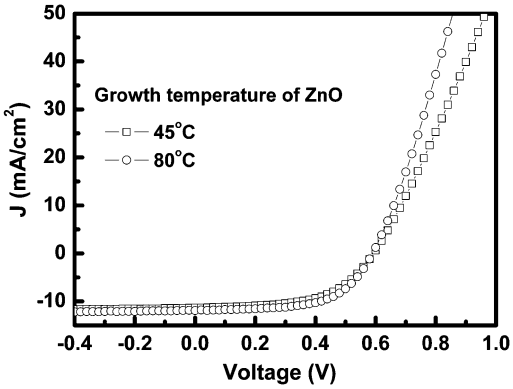

Fig. 5 Comparison of the *J*–*V* curves of the inverted organic solar cells with 36 nm ZnO grown at 45 °C and 80 °C.

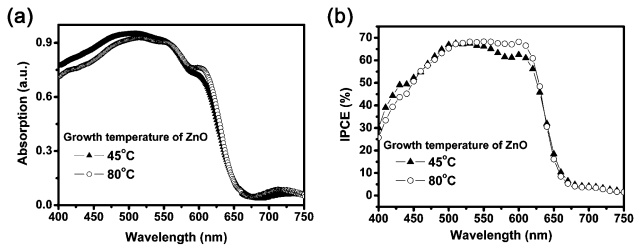

Fig. 6 (a) The absorption and (b) the EQE spectra of the inverted organic solar cells with 36 nm ZnO grown at 45 °C and 80 °C.

of FF as well as the forward current with ZnO thicker than 36 nm is attributed to series resistance. It is also notable that ZnO can also serve as a buffer layer which enhances electron injection from ITO into the active layer at high forward bias. The devices with ZnO of thickness more than 18 nm therefore exhibit diode-like *J*–*V* characteristics.

It was reported that the resistivity of ZnO grown by ALD decreases at higher growth temperatures.[29] Since lower ZnO resistivity is beneficial to the photovoltaic response of solar cells, we repeated the experiments at an elevated temperature. A slightly higher temperature of 80 °C was chosen. Except for the ZnO deposition temperature, all other processing parameters of device fabrication remained unchanged. The measured illuminated *J*–*V* curves of the resulted devices are shown in Fig. 4 and their performance parameters are summarized in Table 2. The *J*–*V* curves exhibit similar trends to those of the devices with ZnO grown at 45 °C, albeit with more diode-like feature for the device with 18 nm ZnO. Similar to the devices with ZnO grown at 45 °C, the FF and PCE reach their maximum at the ZnO thickness of 36 nm and gradually decrease as the thickness of ZnO increases. Comparing Tables 1 and 2 for devices with identical ZnO thicknesses, the devices with ZnO grown at 80 °C show consistently enhanced photovoltaic response. With 36 nm thick film grown at 80 °C, a PCE of 4.18% was achieved, which is the highest PCE for a flexible organic solar cell ever reported in the literature.

Fig. 5 shows the comparison of *J*–*V* curves of devices with 36 nm ZnO grown at 45 °C and 80 °C, respectively. The absorption and EQE spectra of these two devices are also shown in Fig. 6(a) and (b). It is clear from a comparison of the inverse slope of *J*–*V* curve at V_{oc} from Fig. 5 that the series resistance of the device with ZnO grown at 80 °C is smaller than that grown at 45 °C. The FF and PCE are therefore improved for the device with ZnO grown at 80 °C. It is noteworthy from Fig. 6(a) that both devices show strong absorption around 400 nm and 600 nm, as compared to similar inverted devices albeit with solution processed ZnO nanoparticles and glass substrates.[15] From Fig. 6(b), an increase in EQE over the range from 550 nm to 625 nm is observed. It is also notable that while the absorption of the OSC with ALD ZnO grown at 80 °C is less than that with ZnO grown at 45 °C from 460 nm to 550 nm (Fig. 6(a)), the EQEs for both show no appreciable difference (Fig. 6(b)).

The series resistance is related to the energy loss in carrier transport and is strongly affected by the interfaces across which carriers travel to the electrodes. It is therefore interesting to investigate the effects of ZnO growth temperature on its contact to the P3HT : PCBM active layer. AFM morphologies of the ZnO grown at 45 °C and 80 °C were measured and the results are shown in Fig. 7. It is found that the surface morphology of the ZnO is altered when deposited at 80 °C, and the root mean square roughness decreases from 2.13 nm to 1.43 nm. Moreover, the contact angle of ZnO increases from 95° to 100° as the growth temperature increased from 45 °C to 80 °C. The ZnO thin film deposited at 80 °C exhibits therefore a more

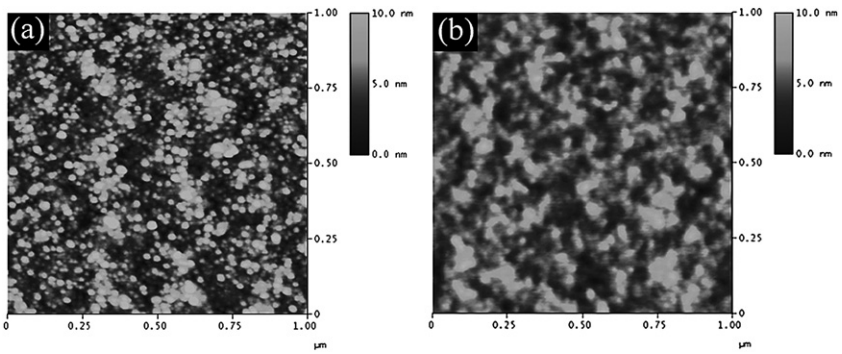

Fig. 7 AFM images of the 36 nm ZnO thin films grown on ITO-coated PEN substrates at (a) 45 °C and (b) 80 °C.

hydrophobic surface which is beneficial to the adhesion of polymer films and leads to reduced series resistance. Improved adhesion also leads to improved interface between the active layer and the ZnO electron selective layer, which in turn results in enhanced electron transport to the ITO electrode and thus enhanced EQE.

In summary, ALD-grown ZnO was used as the electron-selective layer in flexible organic solar cells and a high PCE of 4.18% was achieved at a ZnO deposition temperature of 80 °C. The improvement in photovoltaic response was attributed to the blocking of hole diffusion and an enhanced electron collecting efficiency to the ITO electrode. Since the whole processing temperature can be kept below 110 °C, our inverted organic solar cells are readily compatible with manufacturing on plastic substrates such as PEN.

Acknowledgements

This work was supported by the National Science Council (NSC) of Taiwan, the Republic of China, under grant NSC 97-2120-M-007-004 and NSC 98-2628-M-009-001.

References

1 W. Ma, C. Yang, X. Gong, K. Lee and A. J. Heeger, *Adv. Funct. Mater.*, 2005, **15**, 1617.
2 S. S. Kim, S. I. Na, J. Jo, G. Tae and D. Y. Kim, *Adv. Mater.*, 2007, **19**, 4410.
3 B. C. Thompson and J. M. J. Fréchet, *Angew. Chem., Int. Ed.*, 2008, **47**, 58.
4 M. Jørgensen, K. Norrman and F. C. Krebs, *Sol. Energy Mater. Sol. Cells*, 2008, **92**, 686.
5 R. Kroon, M. Lenes, J. C. Hummelen, P. W. M. Blom and B. de Boer, *Polym. Rev.*, 2008, **48**, 531.
6 F. C. Krebs, *Sol. Energy Mater. Sol. Cells*, 2009, **93**, 394.
7 H. H. Liao, L. M. Chen, Z. Xu, G. Li and Y. Yang, *Appl. Phys. Lett.*, 2008, **92**, 173303.
8 J. Huang, G. Li and Y. Yang, *Adv. Mater.*, 2008, **20**, 415.
9 Y. F. Lim, S. Lee, D. J. Herman, M. T. Lloyd, J. E. Anthony and G. G. Malliaras, *Appl. Phys. Lett.*, 2008, **93**, 193301.
10 L. M. Chen, Z. Hong, G. Li and Y. Yang, *Adv. Mater.*, 2009, **21**, 1.
11 Z. Xu, L. M. Chen, G. Yang, C. H. Huang, J. Hou, Y. Wu, G. Li, C. H. Hsu and Y. Yang, *Adv. Funct. Mater.*, 2009, **19**, 1.
12 C. Waldauf, M. Morana, P. Denk, P. Schilinsky, K. Coakley, S. A. Choulis and C. J. Brabec, *Appl. Phys. Lett.*, 2006, **89**, 233517.
13 C. Y. Li, T. C. Wen, T. H. Lee, T. F. Guo, J. C. A. Huang, Y. C. Lin and Y. J. Hsu, *J. Mater. Chem.*, 2009, **19**, 1643.
14 A. K. K. Kyaw, X. W. Sun, C. Y. Jiang, G. Q. Lo, D. W. Zhao and D. L. Kwong, *Appl. Phys. Lett.*, 2008, **93**, 221107.
15 S. K. Hau, H. L. Yip, N. S. Baek, J. Zou, K. O'Malley and A. K. Y. Jen, *Appl. Phys. Lett.*, 2008, **92**, 253301.
16 F. C. Krebs, *Sol. Energy Mater. Sol. Cells*, 2008, **92**, 715.
17 F. C. Krebs, S. A. Gevorgyan and J. Alstrup, *J. Mater. Chem.*, 2009, **19**, 5442.
18 F. C. Krebs, S. A. Gevorgyan, B. Gholamkhass, S. Holdcroft, C. Schlenker, M. E. Thompson, B. C. Thompson, D. Olson, D. S. Ginley, S. E. Shaheen, H. N. Alshareef, J. W. Murphy, W. J. Youngblood, N. C. Heston, J. R. Reynolds, S. Jia, D. Larid, S. M. Tuladhar, J. G. A. Dane, P. Atienzar, J. Nelson, J. M. Kroon, M. M. Wienk, R. A. J. Janssen, K. Tvingstedt, F. Zhang, M. Andersson, O. Inganäs, M. Lira-Cantu, R. de Bettignies, S. Guillerez, T. Aernouts, D. Cheyns, L. Lutsen, B. Zimmermann, U. Würfel, M. Niggemann, H. F. Schleiermacher, P. Liska, M. Grätzel, P. Lianos, E. A. Katz, W. Lohwasser and B. Jannon, *Sol. Energy Mater. Sol. Cells*, 2009, **93**, 1968.
19 F. C. Krebs, *Org. Electron.*, 2009, **10**, 761.
20 R. L. Puurunen, *J. Appl. Phys.*, 2005, **97**, 121301.
21 W. J. Potscavage, S. Yoo, B. Domercq and B. Kippelen, *Appl. Phys. Lett.*, 2007, **90**, 253511.
22 M. Knez, K. Nielsch and L. Niinistö, *Adv. Mater.*, 2007, **19**, 3425.
23 E. Katsia, N. Huby, G. Tallarida, B. Kutrzeba-Kotowska, M. Perego, S. Ferrari, F. C. Krebs, E. Guziewicz, M. Godlewski, V. Osinniy and G. Luka, *Appl. Phys. Lett.*, 2009, **94**, 143501.
24 M. Vogel, S. Doka, Ch. Breyer, M. Ch. Lux-Steiner and K. Fostiropoulos, *Appl. Phys. Lett.*, 2006, **89**, 163501.
25 M. Glatthaar, M. Riede, N. Keegan, K. Sylvester-Hvid, B. Zimmermann, M. Niggemann, A. Hinsch and A. Gombert, *Sol. Energy Mater. Sol. Cells*, 2007, **91**, 390.
26 F. C. Krebs and K. Norrman, *Progr. Photovolt.: Res. Appl.*, 2007, **15**, 697.
27 Y. X. Wang, S. R. Tseng, H. F. Meng, K. C. Lee, C. H. Liu and S. F. Horng, *Appl. Phys. Lett.*, 2008, **93**, 133501.
28 C. Tao, S. Ruan, X. Zhang, G. Xie, L. Shen, X. Kong, W. Dong, C. Liu and W. Chen, *Appl. Phys. Lett.*, 2008, **93**, 193307.
29 E. Guziewicz, I. A. Kowalik, M. Godlewski, K. Kopalko, V. Osinniy, A. Wojcik, S. Yatsunenko, E. Lusakowska, W. Paszkowicz and M. Guziewicz, *J. Appl. Phys.*, 2008, **103**, 033515.

